geosciences

MDPI

Article

Heavy Minerals Distribution and Provenance in Modern Beach and Fluvial Sands of the Betic Cordillera, Southern Spain

Anna Chiara Tangari [1,2,*], Daniele Cirillo [2,3], Raffaella De Luca [4], Domenico Miriello [5], Elena Pugliese [5] and Emilia Le Pera [5]

[1] Civil Engineering Department (DINCi), University of Calabria, 87036 Arcavacata di Rende, Italy
[2] Science Department, University of Chieti-Pescara, 66100 Chieti, Italy; daniele.cirillo@unich.it
[3] Laboratory of Structural Geology, 3D Digital Cartography and Geomatics, University of Chieti-Pescara, 66100 Chieti, Italy
[4] Direzione Regionale Musei Calabria, Palazzo Arnone, Via Gian Vincenzo Gravina, 87100 Cosenza, Italy; raffaella.deluca@cultura.gov.it
[5] Biology, Ecology and Earth Sciences Department (DiBEST), University of Calabria, 87036 Arcavacata di Rende, Italy; domenico.miriello@unical.it (D.M.); elena.pugliese@unical.it (E.P.); emilia.lepera@unical.it (E.L.P.)
* Correspondence: a.tangari@unich.it

Abstract: This study uses heavy detrital minerals to determine actualistic fluvial and beach sand provenance across the Betic Cordillera (Spain), along the coast from Almeria to Marbella. The Betic Cordillera, primarily composed of metamorphic rocks to the east, supply an assemblage dominated by almandine and graphite, with a longshore dispersal from Almeria to Malaga. Buergerite and hypersthene indicate the provenance of calcalkaline lavas east of Cabo de Gata. The western part of the Betic Cordillera, which comprises the Ronda Peridotite Complex, supplies a chromite and diopside assemblage, with a dispersal from Marbella to Algeciras. Considering these mineralogical suites, the effects of source rock compositions and weathering are evaluated. The heavy mineral species mirror the mineralogy of the source rocks of local outcrops and wider source terranes. The fluvial heavy mineral suites do not differ significantly from those in the beaches except for some unstable species. Unstable species such as olivine, pyroxene, and amphibole do not show evidence of loss because of elevated topography and semiarid climate, which do not affect heavy minerals. This contribution also evaluates the potential of some heavy detrital species as ideal pathfinders in searching for diamonds.

Keywords: Betic Cordillera; modern sands; heavy minerals; provenance

Citation: Tangari, A.C.; Cirillo, D.; De Luca, R.; Miriello, D.; Pugliese, E.; Le Pera, E. Heavy Minerals Distribution and Provenance in Modern Beach and Fluvial Sands of the Betic Cordillera, Southern Spain. *Geosciences* **2024**, *14*, 208. https://doi.org/10.3390/geosciences14080208

Academic Editors: Jesus Martinez-Frias, Lev V. Eppelbaum, Franz Neubauer and Yongjiang Liu

Received: 1 June 2024
Revised: 23 July 2024
Accepted: 2 August 2024
Published: 5 August 2024

1. Introduction

It is well known that the integration of framework composition and heavy minerals of modern sands has revealed an important source of information for provenance determination and has proven to be a useful tool in determining to what extent clastic detritus reflects the signature of parent rocks and the effects of source lithologies and textures, climate, weathering, transport, and depositional environments before diagenetic processes obliterate these features (e.g., [1]). Accordingly, these studies have significantly increased in number [2–8]. This research analyzes and interprets the mineralogy of the heavy minerals of modern sands sampled along a nearly 320 km stretch of the Mediterranean coast of Spain from Almeria to Cadiz (Figure 1a). The exposed lithologies belong to the Betic Cordillera, which has a wide spectrum of source rock types and supplies large amounts of detritus to the coastal and deep-marine environments of the Alboran Sea [9]. The Betic Cordillera, located in southwestern Spain, is an Alpine orogenic thrust belt consisting of several tectono-stratigraphic thrust units, including metamorphic (low- to high-grade), mantle-exhumed rocks (peridotite complex), sedimentary rocks (carbonate, siliciclastic, and evaporite), and volcanic rocks (e.g., [9]). A previous study [10] showed the main

mineralogy of river, beach and offshore sands collected along this margin between Almeria and Cadiz. The authors identified the composition of the sand grains, recognizing three petrologic provinces characterized by distinct detrital modes on the analyzed onshore and offshore sand. These three compositional provinces are Almeria–Malaga Province, Marbella Province, and Almeria–Malaga Province (Figure 1b). The present paper represents a further extension of the previous work because the integration of light and heavy minerals of modern sands has been revealed as an important source of information for provenance determination (e.g., [6,7,11]). The main goals of this study can be summarized as follows:

1. To differentiate heavy mineral assemblages supplied from different source rocks and assessing the utility of heavy minerals as provenance indicators;
2. To quantify the degree to which weathering has potentially reduced heavy minerals' diversity;
3. To determine the role of heavy mineral species as tracers in diamond exploration.

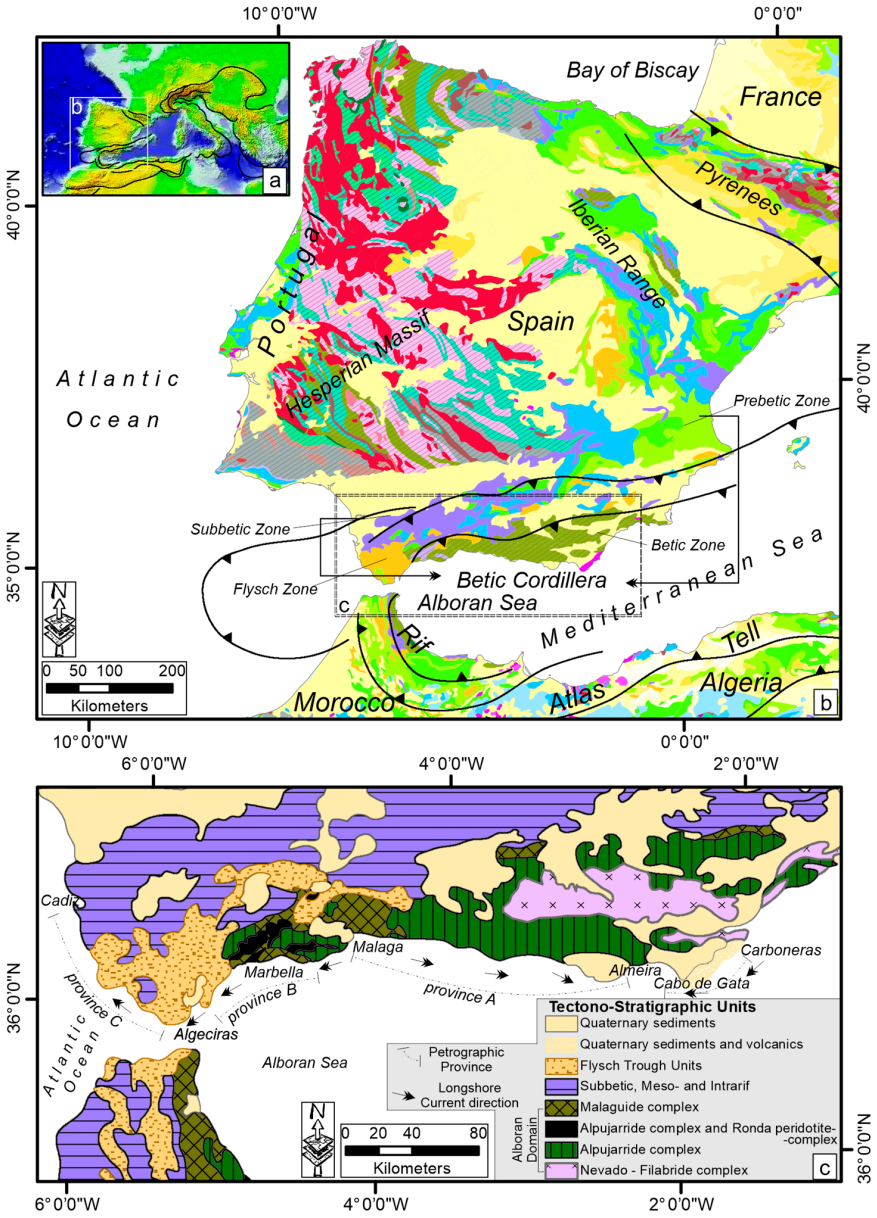

Figure 1. (**a**) Location map of the Iberian Peninsula and northwestern part of Africa; (**b**) geological map of the Iberian and northwestern sector of Africa modified after [12]; (**c**) tectono-stratigraphic map of southwestern Spain (Betic Cordillera) and northwestern sector of Morocco. The legend of the geological map of panel (**a**) is shown in Supplementary Figure S1 [12].

To quantify sediment supply from rivers and beaches of the Betic Cordillera in southwestern Spain and to characterize mineralogical fingerprints of detritus produced by different source rock lithologies, we studied eight very-fine-grained river and beach sand samples.

The results are intended to add to the database on the petrographic features of fluvial and coastal sedimentation, highlighting the useful contribution of heavy detrital mineralogy analysis of the sand fraction as a powerful research tool. The approach would also be suitable for comparison with the sediment provenance in geological and physiographic settings similar to the Mediterranean area.

2. Geology and Physiography of the Source Area

The Betic Cordillera, located in southwestern Spain, is an Alpine orogenic thrust belt consisting of several tectono-stratigraphic thrust units, including metamorphic (low- to high-grade), exhumed mantle rocks (peridotite complex), volcanic rocks, and sedimentary rocks (evaporite, carbonate, siliciclastic) (e.g., [9]). The same tectonic pile is well exposed surrounding the circum-Mediterranean orogenic belt in the Rif Tell and Calabrian arc [13]. The Betic Cordillera belongs to the Alpine chains surrounding the western Mediterranean area from the Gibraltar Arc to the Calabria–Peloritani Arc [14–17]. The orogenic belt forms an arc-shaped arm, formed from the last stage of Alpine Orogeny (from late Mesozoic to Cenozoic time) caused by the convergence between the African and the Iberian and Eurasian plates [13,18]. The arc shape is in continuity from north to south of the Gibraltar Strait across the Rif Mountains in Morocco, Tell and Atlas in Algeria, and the Italian Peninsula in the Calabrian arc [13]. During the Miocene age, the internal zones of all the circum-Mediterranean orogenic belts were affected by uplift. Consequently, orogenic gravitational collapse was driven from the Plio-Pleistocene to Quaternary period by extensional faults that generated intramountain basins [19–24].

The southern boundary of Iberia includes the Betic Cordillera, which is divided into an external and internal domain to the north and south, respectively, and a Flysch Zone in the west [25]. The external domain includes the Prebetic and Subbetic Zone (Figure 1a–c). The Flysch Zone emerges in the Gibraltar Promontory, including quartzose turbidite sequences and claystones from the Cretaceous to the lower Miocene [26]. The internal domain, known as the Betic Zone or Alboran Domain, consists of layered thrust sheets of metasedimentary and sedimentary rocks with an age ranging from the Paleozoic to the Cenozoic (Figure 1a–c). This domain is divided into two main geological units: the Higher Betic Nappe and the Nevado–Filabride Complex. The latter comprise Paleozoic mica schists with garnet and chloritoid–garnet, quartzite, andalusite, cordierite, sillimanite, and garnet gneiss [27]. They also include mica schists, marble, calc-schist, albite-epidote amphibolite, metavolcanic rocks, and serpentinites from the Paleozoic to Triassic periods, along with calcareous breccias and dolostones of a Triassic age [9]. The Nevado–Filabride Complex is covered by the Higher Betic Nappe, mainly represented by two thin thrust sheets: the Malaguide complexes and Alpujarride. (e.g., [28]). In some areas, the Nevado–Filabride Complex separates the Alpujarride Complex via Triassic metasedimentary terranes, referred to as the Almagride Complex. The Alpujarride Complex has Paleozoic quartzite, (possibly pre-Silurian) epidote schist, garnet-bearing schist, mica schist, and marble. It also includes Permian to Triassic phyllite, quartzite, and graphite-bearing and garnet-bearing schist with interbedded marble and metabasalt, as well as Triassic gypsum, limestone, and dolostone [27]. The Alpujarride Complex features the Ronda Peridotite Complex, the most extensively known exposure of upper-mantle rocks worldwide. This complex includes olivine gabbro, peridotite, and spinel or garnet pyroxenite [29], with minimal alteration due to serpentinization [9,27]. The Malaguide Complex comprises non-metamorphosed to very-low-grade metamorphic carbonate rocks, shale, sandstone, conglomerate, gypsum, and chert, with Silurian of an early Miocene age. The tectonic units of the Higher Betic Nappe are unconformably overlayed by clastic, evaporite rocks, and carbonate from the early Miocene to the Quaternary period. Additionally, some outcrops of Miocene (7–15 Ma)

calc-alkaline volcanic and volcaniclastic rocks (andesite to rhyolite) crop out in the area of the coast from Carboneras to Cabo de Gata (Figure 1; [9]).

In the paper by Critelli et al. [10], the mineralogy of beach and river sands collected along the Mediterranean coast side of the Betic thrust belt between Cadiz and Almeria was studied. The composition of the sand grains allowed the authors to recognize three different petrologic provinces characterized by three distinct detrital modes (Figure 1). The latter correspond from west to east with the physiographic provinces of the Malaga Mountains, Sierra Nevada, and Sierra de los Filabres, renamed by Critelli et al. [10] as follows:

1. Algeciras–Cadiz Province (quartzose petrofacies);
2. Marbella Province (quartzolithic ultramaficlastic petrofacies);
3. Almeria–Malaga Province (quartzolithic metamorphic—sedimentaclastic petrofacies).

In the Cabo de Gata–Carboneras province, only one sand sample (381) is volcaniclastic, and Critelli et al. [10] have described it as being without a formal definition of a petrographic province.

The elevation of the Betic Cordillera ranges from sea-level to 3478 m, with the higher altitude corresponding to Mount Mulhacen. The northeast-to-southwest segment of the chain includes a nearly continuous alignment of highlands nearly parallel to the coastline [10]. The drainage of the chain is to the northwest and the south, and the drainage network consists of local and ephemeral drainages (Figure 2), generally less than 50 km in length, delivering clastic supply to the coast. These streams produce occasional catastrophic floods, transporting rapid sediment to the coast and distributing drift currents along the shore. An inverse relationship has been found between sediment discharge and the extent of the drainage basins due to the capacity of the rivers to react to sudden floods and the absence of areas in the drainage basins where sediments could be stored (e.g., [30]). Currently, the climate along the coast varies from semiarid to desert [31], becoming more arid eastward, with a mean annual precipitation of less than 200 mm, and more humid westward, with a value of nearly 1000 mm. The mean annual temperature isotherm along the coast averages at 18 °C [31]. According to these climatic parameters, the weathering efficiency is mainly controlled by mechanical erosion. [1]. Consequently, the sand composition may accurately reflect parent rock compositions of the source region without the depletion of unstable minerals in sediments (e.g., [32]). Littoral drift redistributes sediments on narrow, steep beaches, and storm waves can activate a very active surf zone, inducing powerful littoral drift in both the eastern and western directions (e.g., [33]). Specifically, a prevailing eastward littoral drift predominates between Malaga and Almeria, whereas a westward littoral drift characterizes the coastal stretch from Malaga to Cadiz (Figure 1c) [34]. Not all the continental clastic supply remains on the shelf because the narrowness of the northern Alboran continental shelf likely favors a quick transfer to deeper sedimentary environments (e.g., [30]).

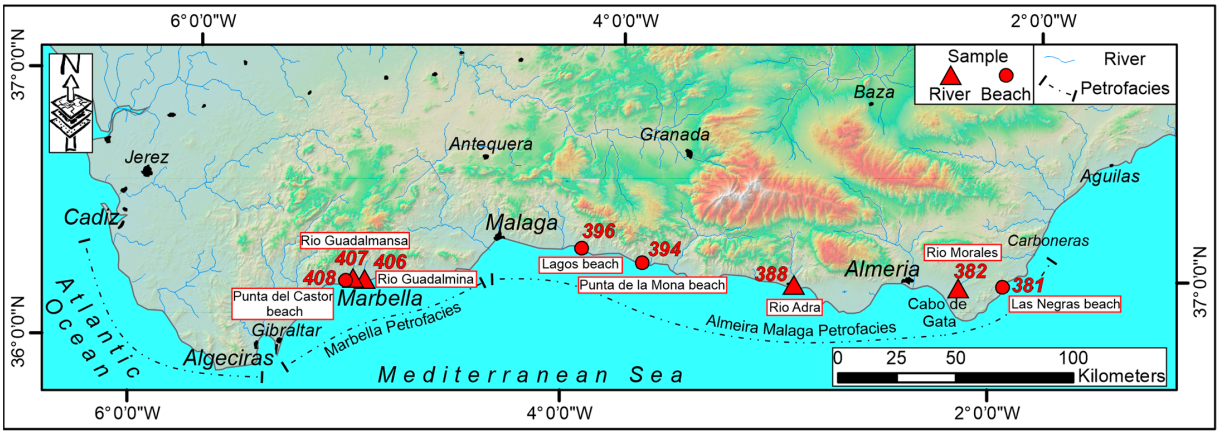

Figure 2. Location map of the sample sites and name of the localities. Triangle: river samples; circle: beach samples.

3. Materials and Methods

We studied eight very-fine-grained river and beach sand samples (Figure 2, Supplementary Table S1).

We collected four samples from the active main channel and bars in the inner reaches of river channels and high-tide berms at four beach localities (e.g., [10]).

These have been analyzed previously for their light mineralogy [10].

The sand was sieved to obtain 3–4 Φ granulometric fractions. These fractions of the sand samples were employed for heavy mineral separation using gravity settling in bromoform, which shows a density of 2.89 g/cm^3 at 20 °C. Magnetite was removed magnetically using a bar magnet, while the remaining heavy minerals were concentrated by passing the fraction multiple times through a Frantz Isodynamic magnetic separator (University Complutense, Madrid, Spain). This procedure concentrated the heavy minerals into five electromagnetic fractions (0.2; 0.5; 1.0; 1.5 and >1.5 A), facilitating their identification [35]. Heavy minerals were mounted on a slide for mineralogical analyses and were analyzed through Raman spectroscopy (University of Calabria, Arcavacata di Rende, Italy). We used this analytical instrumentation because it can be applied to thin sections and grain mounts without requiring any special preparation, unlike other mineralogical analytical tools such as X-ray diffraction [36,37]. We analyzed 50 grains for each electromagnetic fraction. Raman spectra were directly obtained by focusing the laser beam on the grain surface. Micro-Raman analysis was carried out using a Thermo Fisher DXR Raman microscope (Waltham, MA, USA), equipped with OMNICxi Raman Imaging software 1.0, with an objective of 50×, a grating of 900 ln/mm (full width at half maximum, FWHM), and an electron-multiplying charge-coupled device (EMCCD). A 532.0 nm line (solid-state laser) was used at an incident power output ranging from 1.8 to 7 mW. The spatial resolution of the laser beam was 3–5 µm. The spectra acquisition time ranged from 5 to 40 s [38]. The Raman spectra were acquired at a low wavenumber range from ~100 cm^{-1} to 1500 cm^{-1}.

Detrital heavy minerals were identified using a comparison between the obtained Raman peaks and the reference spectra reported in the literature (e.g., [39–62]) and mineralogical databases (http://www.rruff.info, accessed on 31 May 2024) [63].

Heavy mineral grains of nine selected samples were contained only in the 0.2 A, 0.5 A, and 1.0 A fractions. (Table 1). The percentage of heavy minerals in each sample was calculated by considering all the grains in all magnetic fractions.

Table 1. Distribution of heavy minerals in the different electromagnetic Franz fractions of each petrofacies. Alm = almandine; Hyp = hypersthene; Aug = Augite; Di = Diopside; Omp = omphacite; Hbl = hornblende; Krs = kaersutite; Tr = tremolite; Cum = cummingtonite; Act = actinolite; Ep = epidote; Bur = buergerite; St = staurolite; Cld = chloritoid; Sill = Sillimanite; Fo = forsterite; Chr = chromite.

Samples	Petrofacies	Sample Environment	Electromagnetic Fraction (A)	Heavy Minerals
382 Rio Morales	*A: Almeria-Malaga*	fluvial	1.0	Ep + Bur
			0.5	Alm + Cld + Bur
388 Rio Adra		fluvial	1.0	Ep
			0.5	Alm
381 Las Negras beach		beach	0.5	Bur + Hbl + Cum + Hyp + Aug + Di + Omp
			0.2	Hyp + Krs + Bur
394 Punta de la Mona beach		beach	1.0	St + Sill
			0.5	Alm + Tr + Mnz
396 Lagos beach		beach	1.0	Tr + St
			0.5	Alm + Di

Table 1. *Cont.*

Samples	Petrofacies	Sample Environment	Electromagnetic Fraction (A)	Heavy Minerals
406 Rio Guadalmina	*B: Marbella*	fluvial	0.5	Fo + Hyp + Act
			0.2	Chr
407 Rio Guadalmansa		fluvial	1.0	Fo + Aug + Di
			0.5	Alm + Di + Fo + Chr
408 Punta del Castor beach		beach	1.0	Fo + Hyp + Aug + Act
			0.5	Alm + Di + Cum

4. Results

Each sedimentary petrofacies in the Betic Cordillera orogen generates siliciclastic sediment with a specific detrital signature for light (e.g., [10]) and heavy detrital mineralogy.

The results of the Raman analysis are shown in Figures 3–6. The heavy mineral suites observed in Almeria–Malaga and Marbella petrofacies mainly include pyroxene, amphibole, and garnet (Figures 3, 4 and 5a). The main difference in composition is shown by the presence of metasedimentary heavy minerals (Figure 5b–d), epidote (Figure 5e), tourmaline (Figure 5f), and monazite (Figure 6a) in the Almeria–Malaga petrofacies. At the same time, actinolite, olivine, and spinel characterize the Marbella petrofacies (Figure 6b–d).

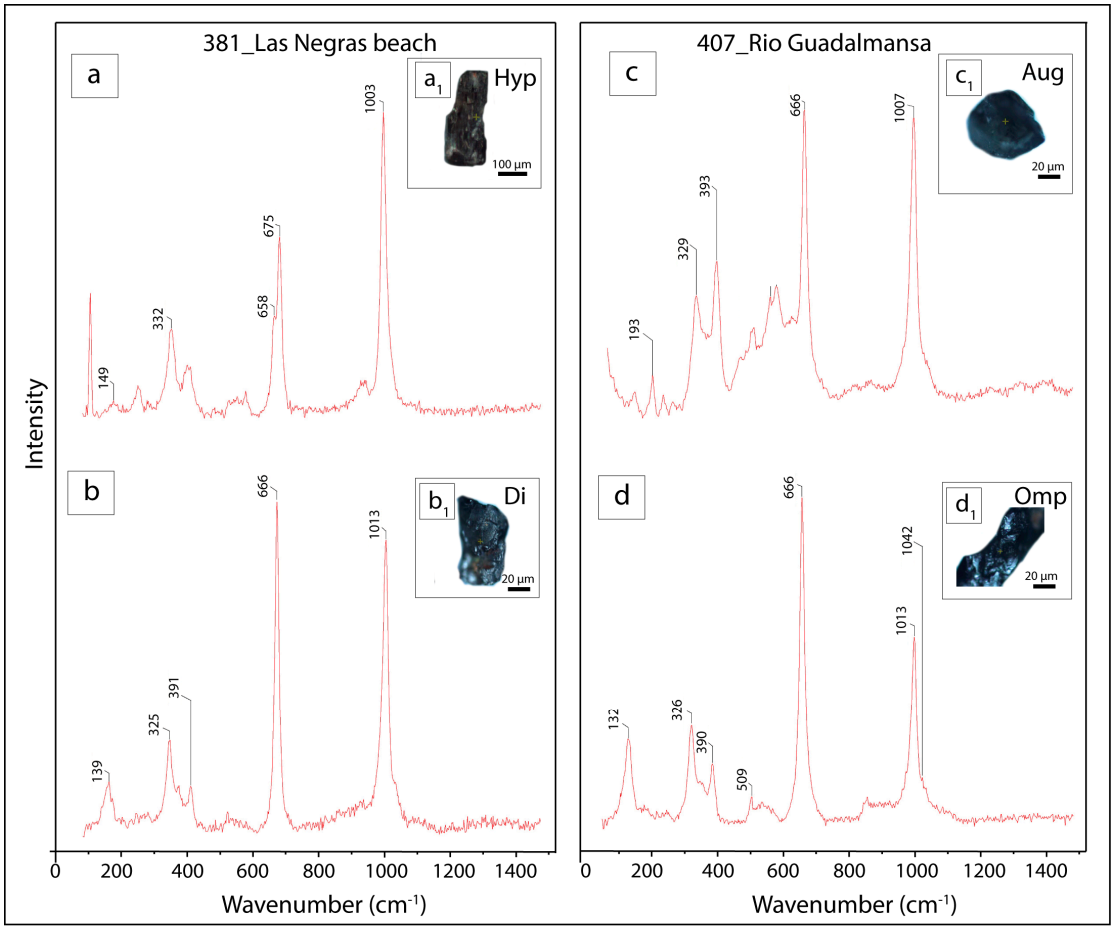

Figure 3. Raman spectra of pyroxene in the Almeria–Malaga petrofacies. (**a**) Hypersthene (Hyp) and (**b**) diopside (Di) in Las Negras beach; (**c**) Augite (Aug) and (**d**) omphacite (Omp) occurring in Rio Guadalmansa.

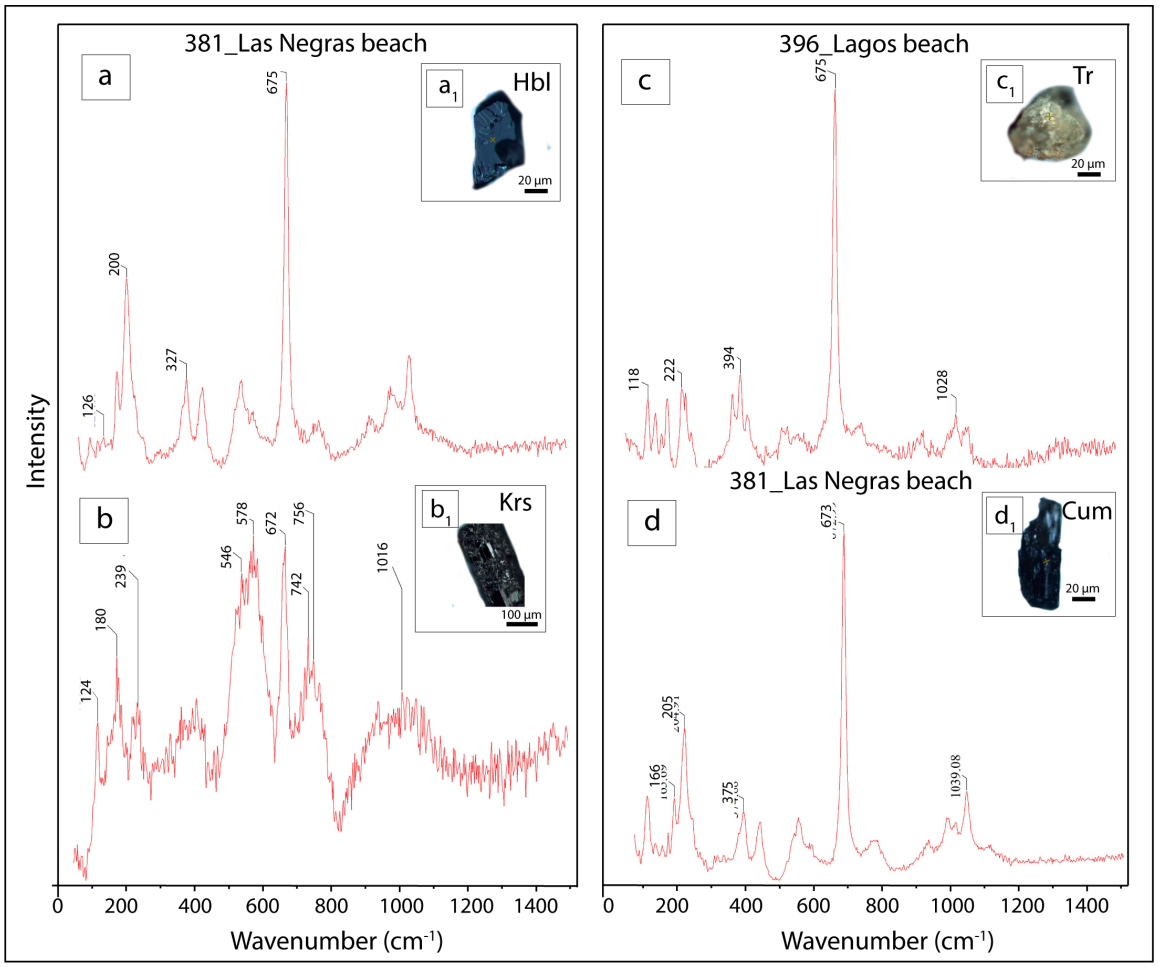

Figure 4. Raman spectra of amphibole in the Almeria–Malaga petrofacies. (**a**) Hornblende (Hbl) and (**b**) kaersutite (Krs) detected in Las Negras beach; (**c**) tremolite (Tr) occurring in the Lagos beach; (**d**) cummingtonite (Omp) identified in Las Negras beach.

Pyroxene includes orthopyroxene, hypersthene (Figure 3a), and clinopyroxene as diopside, augite, and omphacite (Figure 3b–d).

Amphiboles are characterized by hornblende, kaersutite, tremolite, and cummingtonite in the Almeria–Malaga petrofacies (Figure 4a–d) and by actinolite in the Marbella petrofacies (Figure 6b).

Garnet is characterized by almandine (Figure 5a), which is often in association with graphite (Figure 7).

Metasedimentary heavy minerals include staurolite (Figure 5b), chloritoid (Figure 5c), and sillimanite (Figure 5d). Tourmaline is characterized by diagnostic bands [39,44] confirming the presence of the buergerite variety (Figure 5f).

The Marbella petrofacies is also composed of olivine as forsterite (Figure 6c) and spinel as chromite (Figure 6d).

All the heavy minerals are primarily characterized by morphological features indicative of mechanical weathering.

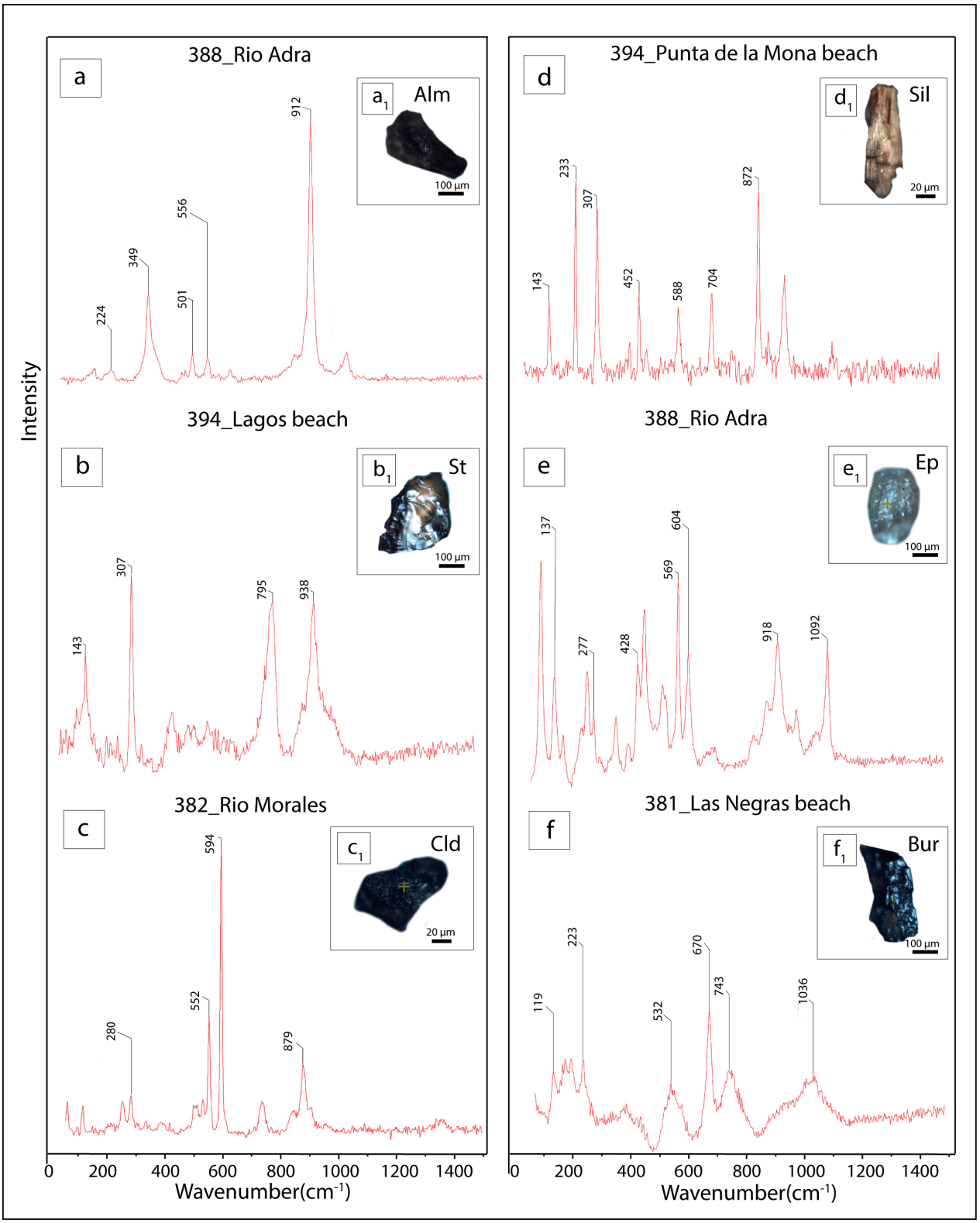

Figure 5. Raman spectra of heavy minerals detected in Almeria–Malaga petrofacies. (**a**) Garnets such as almandine (Alm) identified in Rio Adra, (**b**) staurolite (St) detected in Lagos beach; (**c**) chloritoid (Cld) occurring in Rio Morales; (**d**) sillimanite (Sil) identified in Punta de la Mona beach; (**e**) epidote (Ep) identified in Rio Adra; (**f**) tourmaline detected as buergerite (Bur) in Las Negras beach.

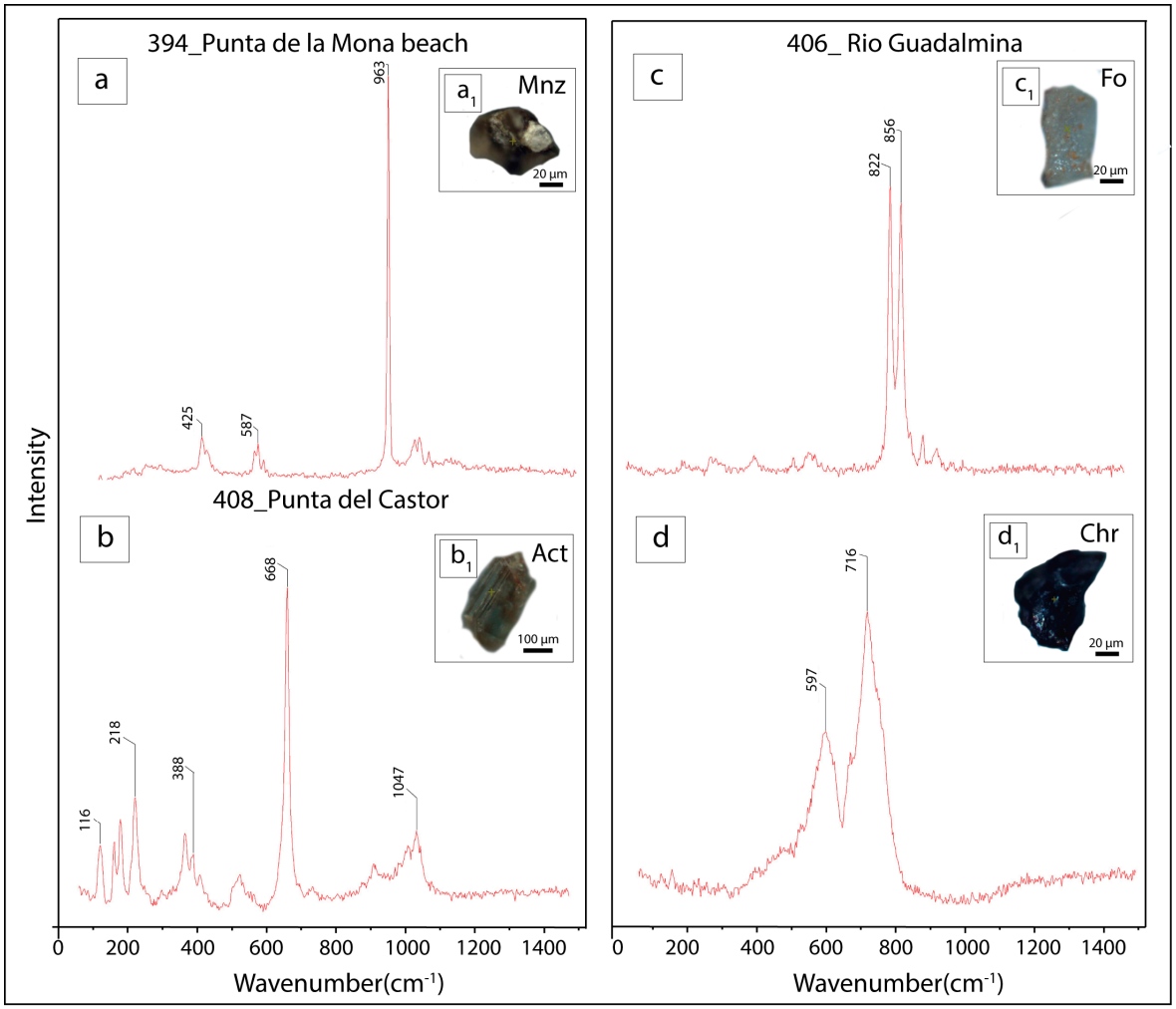

Figure 6. Raman spectra of heavy minerals in Almeria–Malaga and Marbella petrofacies, respectively. (**a**) Monazite (Mnz) in Punta del la Mona beach; (**b**) actinolite (Act) detected in Punta del Castor; (**c**) forsterite-type (Fo) olivine and (**d**) chromite (Chr) in Rio Guadalmina.

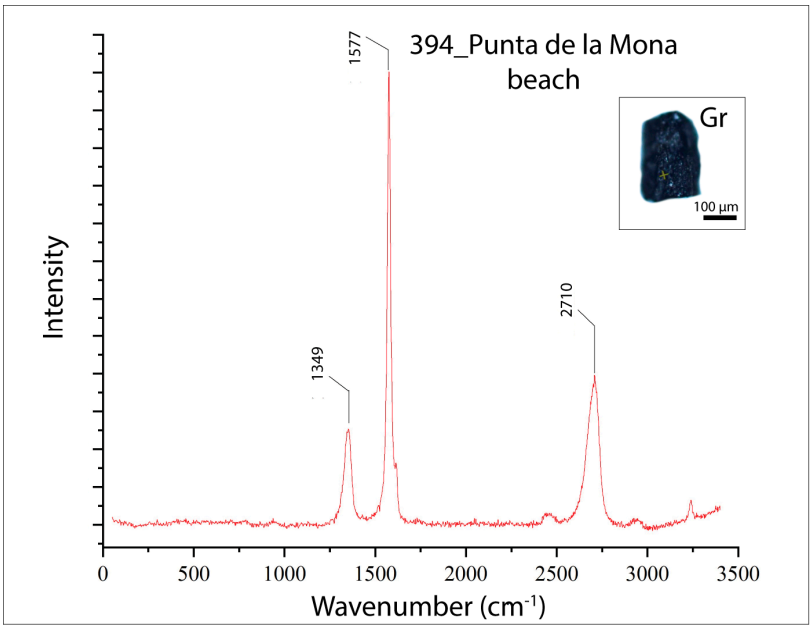

Figure 7. Raman spectrum of graphite in Punta de la Mona beach, in the Almeria–Malaga petrofacies.

4.1. Distribution of Heavy Minerals in the Almeria-Malaga Petrofacies

Heavy minerals are concentrated in different electromagnetic Franz fractions (Table 1). Tourmaline-type buergerite, augite, and tremolite are mainly concentrated in electromagnetic fractions 1.0 A and 0.5 A. Specifically, buergerite also characterizes the 0.2 A electromagnetic fraction where kaersutite and hypersthene are also present. Hypersthene is also concentrated in the 0.5 A electromagnetic fraction. This fraction also includes almandine, hornblende, cummingtonite, diopside, omphacite, chloritoid, and monazite. Epidote, sillimanite, and staurolite characterize the 1.0 A electromagnetic Frantz fraction.

In this petrofacies, only one sand sample, from Las Negras beach, is volcaniclastic (Cabo de Gata–Carboneras province), and it will be described without a formal definition of the petrographic province. Specifically, this sand sample is composed mainly of the orthopyroxene hypersthene (~24%), the clinopyroxene augite, diopside, and omphacite (~23%), amphibole (29%), and tourmaline (~24%) (Figure 8). Amphiboles include hornblende, kaersutite and cummingtonite. The tourmaline buergerite is also found in an amount of 24%, compared to that in Rio Morales, where this mineral shows a lower abundance of 16% (Figure 8).

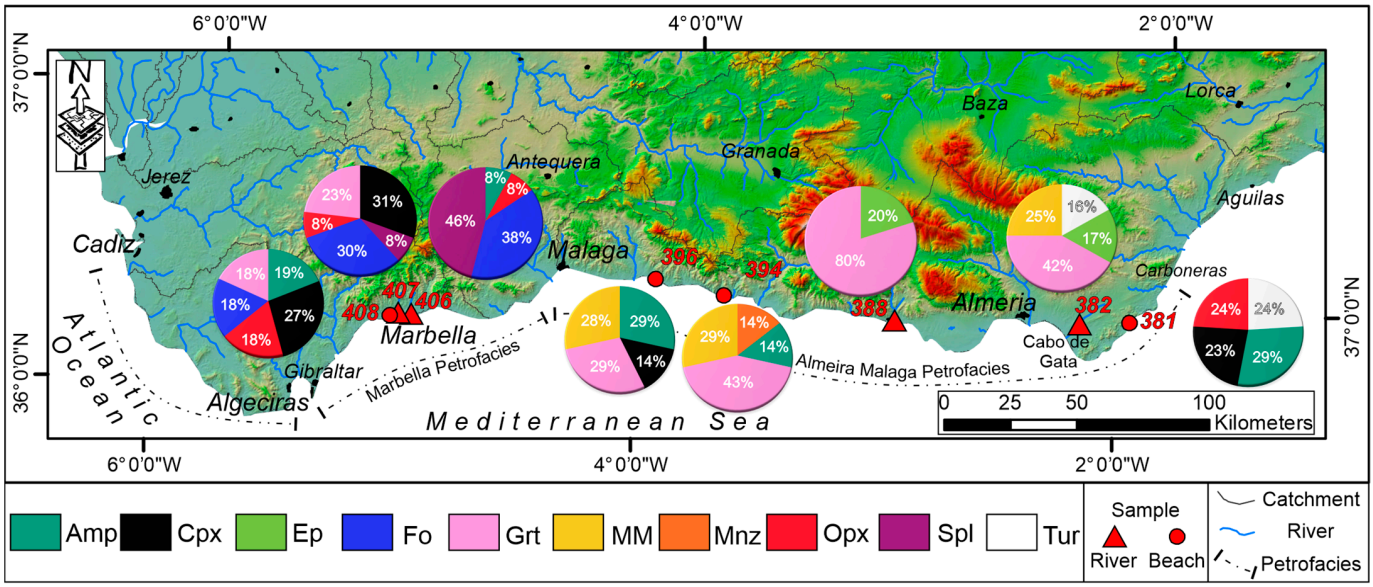

Figure 8. Distribution of heavy mineral percentages in Almeria–Malaga and Marbella petrofacies with the location of the sampling sites. Tur = tourmaline (Bur); Mnz = monazite; Amp = amphibole (Hbl, Cum, Tr, Act); Cpx = clinopyroxene (Di, Aug, Omp); Opx = Orthopyroxene (Hyp); Fo = forsterite; Spl = Spinel; Ep = Epidote; Grt = Garnet (Alm); MM = metasedimentary heavy minerals (St, Cld, Sil).

Different to samples from Las Negras beach, in the other beach samples (Punta de la Mona and Lagos), amphibole is represented by tremolite in amounts of 14% and 29% (Table 1; Figure 8), respectively. These minerals are not present in the Rio Morales and Rio Adra samples (Figure 8). In all sand samples, the amount of garnet, composed of almandine species, ranges from 29% to 80% except in Las Negras beach (Figure 8). In both Punta de la Mona and Lagos beach, this mineral is often in association with graphite. This latter is also present as an inclusion in the garnet of Rio Adra. An average value of about 13% of epidote is detected in Rio Morales and Rio Adra (Figure 8). Metasedimentary heavy minerals (~27%) are observed in Rio Morales with the occurrence of chloritoid and in Punta de la Mona beach and with the presence of staurolite and sillimanite (Figure 8). Staurolite in Lagos beach is also found (Table 1). An amount of 14% of monazite is found in Punta de la Mona beach (Figure 8). Carbonates such as ankerite and dolomite are identified in Rio Morales and Rio Adra.

The surface texture of the heavy minerals suites is fresh and angular and does not show etching processes due to dissolution (Figure 3(a_1,b_1,c_1,d_1); see Figure 4(a_1,b_1,c_1,d_1), Figure 5(a_1,b_1,c_1,d_1,e_1,f_1), and Figure 6(a_1,b_1,c_1,d_1)).

4.2. Distribution of Heavy Minerals in the Marbella Petrofacies

The results of different electromagnetic fractions of Marbella petrofacies are shown in Table 1. These electromagnetic fractions exhibit the concentrations of forsterite, hypersthene, diopside, and actinolite in the 1.0 A and 0.5 A fractions. Moreover, the 0.5 A electromagnetic fraction includes almandine and cummingtonite with respect to the 1.0 A fraction, in which augite and chromite are concentrated. Chromite in the 0.2 A electromagnetic fraction is also observed.

Forsterite occurred in all sand samples, reaching an amount of up to 38% in Rio Guadalmina and decreasing in amount to 18% at Punta del Castor beach (Figure 8). Punta del Castor beach sand hypersthene show a higher value, of about 18%, than the other sand samples.

The river (Rio Guadalmansa) to beach environment transition (Punta del Castor) shows a slight decrease in abundance, ranging from 31% to 27% and 23% to 18%, for diopside, augite, and garnet. Amphiboles is present in higher amounts in Punta del Castor beach (19%) and shows a lower value in the Rio Gualdamina (8%) (Figure 8). Chromite was found in Rio Guadalmina and Rio Guadalmansa (Figure 8).

5. Discussion

5.1. Betic Cordillera Source Rock Types and Heavy Minerals

The efficiencies of the concentrating processes are not the same for each mineral (e.g., [10,64]), and according to their mobility, the occurring heavy mineral assemblages indicate that these were delivered to the beach environment by rivers as bedload (e.g., [65]). In terms of both water discharge and sediment transport, Andalusian river systems are quite efficient despite the small size of their catchments (e.g., [30]).

In this study, many heavy mineral species were recorded: almandine, hypersthene, augite, diopside, omphacite, hornblende, kaersutite, tremolite, cummingtonite, actinolite, epidote, buergerite, staurolite, chloritoid, sillimanite, forsterite, and chromite. This great variety is interpreted because of the weathering-limited erosion regime within the Betic Cordillera, which has not affected the diversity of the heavy mineral assemblages taken into the bedload rivers and transported to the coast. Clastic sedimentation is characterized by unstable minerals such as olivine and pyroxenes in the sand. The high heavy mineral diversity of this study area demonstrated that they have value as sensitive indicators of both a local and broader scale of provenance. For example, the Rio Morales and Las Negras beach heavy mineral assemblages reflect a restricted outcrop of volcanic rocks at the Cabo de Gata promontory. The main heavy species are buergerite, augite, and hypersthene. Specifically, buergerite was first found in hydrothermally altered tuffs and clayey rhyolites near Mexquitic, San Luis Potosi, Mexico [66], in aplite–pegmatite veins of the Plana Cretaceous Pluton in Bulgaria [67] and as a detrital mineral in Paleozoic felsic metasedimentary source rocks [68]. The mineral suites also reflect variations in the broader scale of provenance from Almeria to Malaga.

The main heavy mineral association of the Almeria–Malaga province is dominated by almandine associated with graphite, which is often present as an inclusion in almandine. Specifically, graphite can be considered a provenance-diagnostic detrital species (e.g., [69]) ascribed to sediment supplies mainly from small outcrops of the graphite-bearing schists of the Alpujarride Complex (Figures 1c and 7). The assemblage of sillimanite, staurolite, almandine, chloritoid, monazite, and epidote are ascribed to provenance from the Nevado–Filabride Complex metamorphic rocks (Figures 1c and 8). In contrast, the presence of dolomite suggests that this detrital species is supplied by metasedimentary lithotypes of the Nevado–Filabride Complex and the Alpujarride Complexes (Figures 1 and 8). In Marbella Province [10], the Ronda Peridotite Complex, including peridotites, gabbros, and

serpentinites [19], is dominated by olivine as forsterite, chromite, and diopside (Table 1, Figures 1c and 8). Even though the ultramafic rocks of the Ronda Peridotite Complex represent a restricted outcrop area, the abundance of ultramaficlastic heavy species is much higher than that of almandine supplied by the garnet-bearing schists of the Alpujarride Complex (Figures 1 and 8), which has a much wider areal extent in the hinterland. The overrepresentation of the ultramaficlastic detritus can be related to a Sand Generation Index [22] for the Ronda Peridotite Complex that is higher than that of the Nevado–Filabride metamorphites.

Therefore, we can confirm that the mineralogy of the river and beach sands analyzed reflects the provenance of source rocks belonging to the catchment. This correlation between mineralogical data and local geological characteristics enhances our understanding of the study area's sedimentary dynamics and erosion sources (Figure 9a–d).

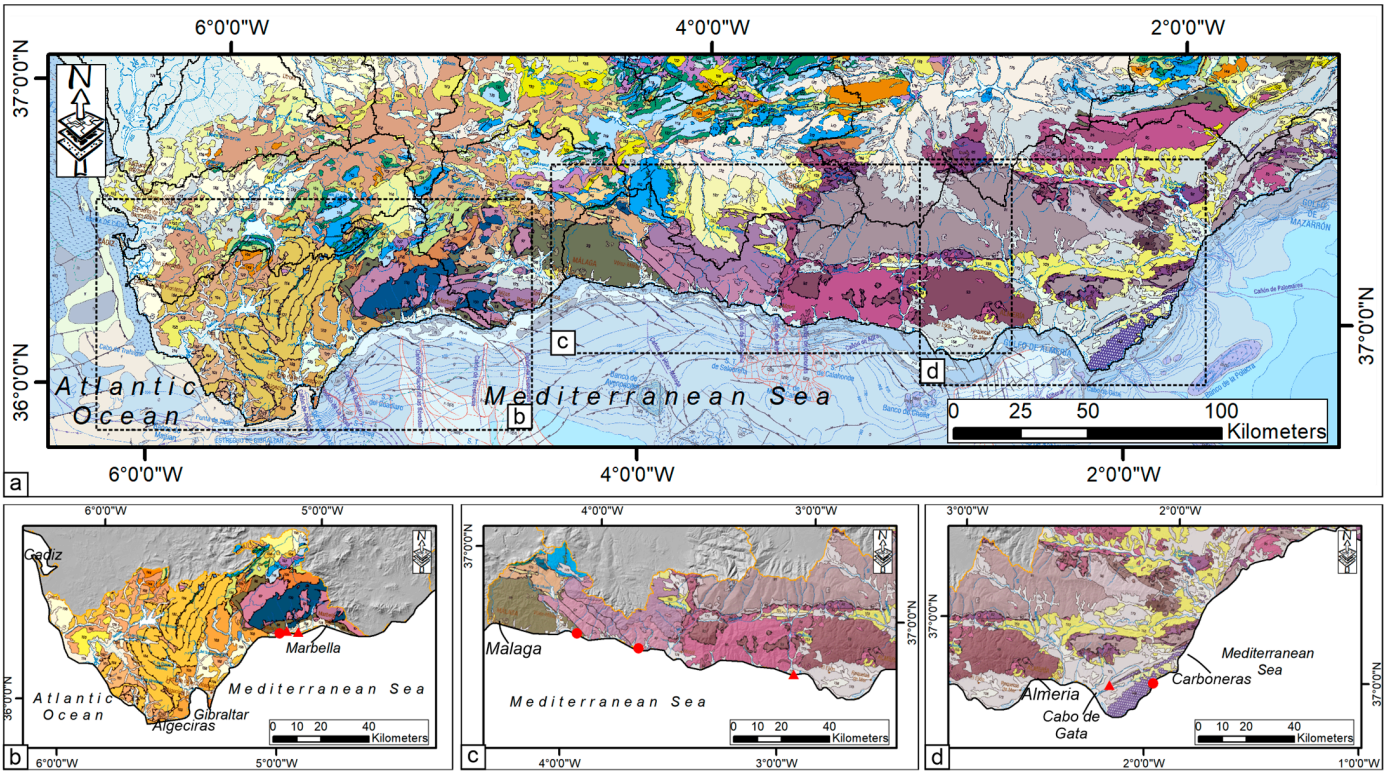

Figure 9. (**a**) Geological map of the southwestern part of the Betic Cordillera (from [64]), with the location sites (black rectangles and square); (**b**) 2D map view of the lithology of Marbella study area with the location sites; (**c**) 2D map view of the lithology of Malaga study area with the location sites; (**d**) 2D map view of the lithology of Almeria site with the location sites. The legend of this map is shown in the Supplementary Figure S2 [70].

5.2. Provenance and Weathering of Heavy Minerals

In the provenance studies is formulated an "order of persistence" of the heavy detrital minerals widely used as a measure of mineral stability in sediments (e.g., [71]). Unstable species include andalusite + pyroxenes + amphiboles (*APA sensu* [11]), epidote + zoisite + kyanite + sillimanite + titanite + brookite (*EKS sensu* [11]) are considered moderately stable, garnet + apatite + staurolite (*GAS sensu* [11]) is regarded as stable, and zircon + tourmaline + rutile are considered ultrastable species (e.g., *ZTR sensu* [72]). Therefore, different heavy minerals display different responses to weathering [5]. This study suggests that the effects of chemical and biochemical weathering on the heavy minerals assemblages have been negligible and that mechanical weathering has also been only a modest cause of compositional modification during transport [73].

5.3. The Role of Tracer Heavy Minerals in Diamond Exploration

The disaggregation of mantle rocks yields large quantities of mantle minerals, commonly referred to as kimberlitic indicator minerals, and, from an exploration point of view, the most important indicator minerals are garnet, chromite, Cr-diopside and olivine (e.g., [74]). In general, these "kimberlitic indicator minerals" are obviously not unique to kimberlites but also include exhumed mantle peridotites like the Ronda massif. Therefore, kimberlitic indicator minerals can be extracted from medium-to-fine sand in sample surface materials such as soil, stream, and till sediments (e.g., [74–76]). Some heavy detrital species, described by Nowicki et al. [74], have been found in the ultramaficlastic Marbella petrofacies (e.g., [10]), confirming that they are supplied from the Ronda Peridotite Complex, which includes peridotite, olivine gabbro, and spinel or garnet pyroxenite as source rocks (e.g., [9,27,29]). Heavy mineral varieties of Betic sand, associated with mantle rocks of the Ronda Peridotite Complex, include garnet, ilmenite, and chromite. These species, considered stable (e.g., [71]), are particularly useful due to their greater ability to survive weathering in the surface environment [5]; thus, in addition to rare diamond, the disaggregation of mantle rocks yields quantities of other mantle minerals, commonly referred to as kimberlitic indicators.

6. Conclusions

The provenance of the heavy minerals assemblages of the river and beach, from Carboneras to Marbella, located in the Betic Cordillera orogenic terranes, is linked to metamorphic (mainly gneisses and schists), ultramafic (peridotite, olivine gabbro, and spinel or garnet pyroxenite) and calcalkaline volcanic rocks, outcropping in the drainage basins of the Andalusian margin. The eastern Betic Cordillera supplies two assemblages: one widespread and dominated by almandine and graphite, derived from garnet–sillimanite gneiss, forming the larger part of the outcrops, and the other by buergerite and hypersthene, identifying a small outcrop of andesite to rhyolite effusive rocks. The western Betic Cordillera supplies an assemblage dominated by forsterite, chromite, and diopside, closely matching the ultramafic bedrock lithology of the Ronda Peridotite Complex.

The results indicate that the effect of weathering did not influence the heavy mineral suites; even olivine, pyroxene and amphibole, susceptible to chemical loss, are well preserved in the sand, with no sign of corrosion or dissolution. Moreover, some mantle rock-derived heavy minerals, such as garnet, chromite, diopside and olivine, are known as kimberlitic indicator minerals.

Supplementary Materials: The following supporting information can be downloaded at https://www.mdpi.com/article/10.3390/geosciences14080208/s1: Figure S1: Geological map of the Iberian Peninsula and northwestern sector of Africa with a legend; Figure S2: Geological map of the Betic Cordillera (southwestern sector of Spain) with the location sample sites and a related legend. Table S1: Location of sampling sites and year of sampling.

Author Contributions: Conceptualization, E.L.P. and A.C.T.; methodology, A.C.T., E.P., E.L.P., D.M. and R.D.L.; software, D.M., R.D.L. and D.C.; validation, A.C.T., E.L.P., D.M., E.P., R.D.L. and D.C.; formal analysis, E.L.P., D.M. and R.D.L.; investigation, A.C.T., E.L.P., D.M., E.P., R.D.L. and D.C.; data curation, A.C.T., E.L.P. and E.P.; writing—original draft preparation, A.C.T. and E.L.P.; writing—review and editing, A.C.T., E.L.P., D.M., E.P., R.D.L. and D.C.; supervision, A.C.T. and E.L.P. All authors have read and agreed to the published version of the manuscript.

Funding: This research received no external funding.

Data Availability Statement: Data is contained within the article or Supplementary Material.

Acknowledgments: We thank José Arribas, Amparo Tortosa, and Salvatore Critelli for the fieldwork sampling. We thank two anonymous reviewers for their fruitful suggestions and comments, which greatly improved the manuscript.

Conflicts of Interest: The authors declare no conflicts of interest.

References

1. Johnsson, M.J. The system controlling the composition of clastic sediments. In *Processes Controlling the Composition of Clastic Sediments*; Johnsson, M.J., Basu, A., Eds.; Geological Society of America: Boulder, CO, USA, 1993; Volume 284, pp. 1–19.
2. Palomares, M.; Arribas, J. Modern stream sands from compound crystalline sources: Composition and sand generation index. In *Processes Controlling the Composition of Clastic Sediments*; Johnsson, M.J., Basu, A., Eds.; Geological Society of America Special Paper: Boulder, CO, USA, 1993; Volume 284, pp. 313–322.
3. Arribas, J.; Critelli, S.; Le Pera, E.; Tortosa, A. Composition of modern stream sand derived from a mixture of sedimentary and metamorphic source rocks (Henares River Central Spain). *Sediment. Geol.* **2000**, *133*, 27–48. [CrossRef]
4. Le Pera, E.; Arribas, J. Sand composition in an Iberian passive-margin fluvial course: The Tajo River. *Sediment. Geol.* **2004**, *171*, 261–281. [CrossRef]
5. Andò, S.; Garzanti, E.; Padoan, M.; Limonta, M. Corrosion of heavy minerals during weathering and diagenesis: A catalog for optical analysis. *Sediment. Geol.* **2012**, *280*, 165–178. [CrossRef]
6. Garzanti, E.; Canclini, S.; Foggia, F.M.; Petrella, N. Unraveling magmatic and orogenic provenance in modern sand: The back-arc side of the Apennine thrust belt, Italy. *J. Sediment. Res.* **2002**, *72*, 2–17. [CrossRef]
7. Garzanti, E.; Andò, S.; Vezzoli, G.; Dell'Era, D. From rifted margins to foreland basins: Investigating provenance and sediment dispersal across desert Arabia (Oman, UAE). *J. Sediment. Res.* **2003**, *73*, 572–588. [CrossRef]
8. Le Pera, E.; Tangari, A.C.; Marinangeli, L.; Morrone, C.; Riber, L.; Andò, S. Provenance of Modern Sands from Baja California Rivers (Mexico): Petrographic Constraints from Light and Heavy Minerals. *J. Sediment. Res.* **2023**, *93*, 617–641. [CrossRef]
9. Weijermars, R. Geology and Tectonics of the Betic Zone, Se Spain. *Earth-Sci. Rev.* **1991**, *31*, 153–236. [CrossRef]
10. Critelli, S.; Arribas, J.; Le Pera, E.; Tortosa, A.; Marsaglia, K.M.; Latter, K.K. The recycled orogenic sand provenance from an uplifted thrust belt, Betic Cordillera, southern Spain. *J. Sediment. Res.* **2003**, *73*, 72–81. [CrossRef]
11. Ibbeken, N.G.H.; Schleyer, R. *Source and Sediment: A Case Study of Provenance and Mass Balance at an Active Plate Margin (Calabria, Southern Italy)*; Springer: Berlin/Heidelberg, Germany, 1991. [CrossRef]
12. Asch, K. Geology without national boundaries: The 1:5 million international geological map of Europe and adjacent areas: IGME 5000. *Episodes* **2006**, *29*, 39–42.
13. van Hinsbergen, D.J.J.; Torsvik, T.H.; Schmid, S.M.; Matenco, L.C.; Maffione, M.; Vissers, R.L.M.; Gürer, D.; Spakman, W. Orogenic architecture of the Mediterranean region and kinematic reconstruction of its tectonic evolution since the Triassic. *Gondwana Res.* **2020**, *81*, 79–229. [CrossRef]
14. Guerrera, F.; Martinalgarra, A.; Perrone, V. Late Oligocene-Miocene Syn-/-Late-Orogenic Successions in Western and Central Mediterranean Chains from the Betic Cordillera to the Southern Apennines. *Terra Nova* **1993**, *5*, 525–544. [CrossRef]
15. Vitale, S.; Ciarcia, S. Tectono-stratigraphic and kinematic evolution of the southern Apennines/Calabria–Peloritani Terrane system (Italy). *Tectonophysics* **2013**, *583*, 164–182. [CrossRef]
16. Amodio, M.L.; Bonardi, G.; Colonna, V.; Dietrich, D.; Giunta, G.; Ippolito, F.; Liguori, V.; Lorenzoni, F.; Paglionico, A.; Perrone, V.; et al. L'arco calabro-peloritano nell'orogene appenninico-maghrebide [The Calabro-Peloritani Arc during the Apennine-Maghrebide Orogeny]. *Mem. Soc. Geol. It.* **1976**, *17*, 1–60.
17. Filice, F.; Liberi, F.; Cirillo, D.; Pandolfi, L.; Marroni, M.; Piluso, E. Geology map of the central area of Catena Costiera: Insights into the tectono-metamorphic evolution of the Alpine belt in Northern Calabria. *J. Maps* **2015**, *11*, 114–125. [CrossRef]
18. Do Couto, D.; Gorini, C.; Jolivet, L.; Lebret, N.; Augier, R.; Gumiaux, C.; d'Acremont, E.; Ammar, A.; Jabour, H.; Auxietre, J.L. Tectonic and stratigraphic evolution of the Western Alboran Sea Basin in the last 25 Myrs. *Tectonophysics* **2016**, *677*, 280–311. [CrossRef]
19. Brozzetti, F.; Cirillo, D.; Liberi, F.; Piluso, E.; Faraca, E.; De Nardis, R.; Lavecchia, G. Structural style of Quaternary extension in the Crati Valley (Calabrian Arc): Evidence in support of an east-dipping detachment fault. *Ital. J. Geosci.* **2017**, *136*, 434–453. [CrossRef]
20. Lavecchia, G.; de Nardis, R.; Ferrarini, F.; Cirillo, D.; Bello, S.; Brozzetti, F. Regional seismotectonic zonation of hydrocarbon fields in active thrust belts: A case study from Italy. In *Building Knowledge for Geohazard Assessment and Management in the Caucasus and other Orogenic Regions*; Bonali, F.L., Mariotto, F.P., Tsereteli, N., Eds.; Springer: Dordrecht, The Netherlands, 2021; pp. 89–128. [CrossRef]
21. Alfaro, P.; Delgado, J.; de Galdeano, C.S.; Galindo-Zaldívar, J.; García-Tortosa, F.J.; López-Garrido, A.C.; López-Casado, C.; Marín-Lechado, C.; Gil, A.; Borque, M.J. The Baza Fault: A major active extensional fault in the central Betic Cordillera (south Spain). *Int. J. Earth Sci.* **2008**, *97*, 1353–1365. [CrossRef]
22. Balanyá, J.C.; Crespo-Blanc, A.; Díaz-Azpiroz, M.; Expósito, I.; Torcal, F.; Pérez-Peña, V.; Booth-Rea, G. Arc-parallel vs back-arc extension in the Western Gibraltar arc: Is the Gibraltar forearc still active? *Geol. Acta* **2012**, *10*, 249–263. [CrossRef]
23. Stich, D.; Morales, J.; López-Comino, J.Á.; Araque-Pérez, C.; Azañón, J.M.; Dengra, M.Á.; Ruiz, M.; Weber, M. Seismogenic structures and active creep in the Granada Basin (S-Spain). *Tectonophysics* **2024**, *882*, 230368. [CrossRef]
24. Brozzetti, F.; Mondini, A.C.; Pauselli, C.; Mancinelli, P.; Cirillo, D.; Guzzetti, F.; Lavecchia, G. Mainshock Anticipated by Intra-Sequence Ground Deformations: Insights from Multiscale Field and SAR Interferometric Measurements. *Geosciences* **2020**, *10*, 186. [CrossRef]
25. Fallot, P. *Les Cordilléres Bétiques*; Consejo Superior de Investigaciones Cientificas, Instituto de Investigaciones Geologicas Lucas Mallada: Barcelona, Spain, 1948.

26. Gutierrez Mas, J.M.; Martin Algarra, A.; Domínguez Bella, S.; Moral Cardona, J.P. *Introduccion a la Geologıa de la Provincia de Cadiz*; Universidad de Cadiz, Servicio de Publicaciones: Cádiz, Spain, 1991.
27. Lundeen, M.T. Emplacement of the Ronda peridotite, Sierra Bermeja, Spain. *Geol. Soc. Am. Bull.* **1978**, *89*, 172–180. [CrossRef]
28. Criniti, S.; Martín-Martín, M.; Martín-Algarra, A.A. New constraints for the western Paleotethys paleogeography-paleotectonics derived from detrital signatures: Malaguide Carboniferous Culm Cycle (Betic Cordillera, S Spain). *Sediment. Geol.* **2023**, *458*, 106534. [CrossRef]
29. Dickey, J.S.J. Partial fusion products in alpine-type peridotites: Serrania de la Ronda and other examples. *Mineral. Soc. Am.* **1970**, *3*, 33–49.
30. Liquete, C.; Arnau, P.; Canals, M.; Colas, S. Mediterranean river systems of Andalusia, southern Spain, and associated deltas: A source to sink approach. *Mar. Geol.* **2005**, *222*, 471–495. [CrossRef]
31. Koppen, W. Versuch einer Klassifikation der klimate vorzugsweise nach ihren Bezie-hungen zur Pflanzenwelt. *Geogr. Z.* **1901**, *6*, 593.
32. Cavazza, W.; Zuffa, G.G.; Camporesi, C.; Ferretti, C. Sedimentary recycling in a temperate climate drainage basin (Senio River, north-central Italy): Composition of source rock, soil profiles, and fluvial deposits. In *Processes Controlling the Composition of Clastic Sediments: Geological Society of America*; Johnsson, M.J., Basu, A., Eds.; Geological Society of America: Boulder, CO, USA, 1993; Volume 284, pp. 226–247.
33. Malvarez, G.; Navas, F.; del Rio, J.L. Assessment and projections of sediment budget resilience in Marbella, Spain. *Front. Mar. Sci.* **2022**, *9*, 933994. [CrossRef]
34. Molina, R.; Anfuso, G.; Manno, G.; Gracia, P.F.J. The Mediterranean Coast of Andalusia (Spain): Medium-Term Evolution and Impacts of Coastal Structures. *Sustainability* **2019**, *11*, 3539. [CrossRef]
35. Parfenoff, A.; Pomerol, C.; Tourenq, J. *Minerals in Grains: Methods of Study and Determination*; Masson & Cie: Paris, France, 1970; 571p.
36. Marinangeli, L.; Pompilio, L.; Baliva, A.; Billotta, S.; Bonanno, G.; Domeneghetti, M.C.; Fioretti, A.M.; Menozzi, O.; Nestola, F.; Piluso, E.; et al. Development of an ultra-miniaturised XRD/XRF instrument for the in situ mineralogical and chemical analysis of planetary soils and rocks: Implication for archaeometry. *Rend. Lincei-Sci. Fis.* **2015**, *26*, 529–537. [CrossRef]
37. Szopa, K.; Skreczko, S.; Chew, D.; Krzykawski, T.; Szymczyk, A. Multi-Tool (LA-ICPMS, EMPA and XRD) Investigation on Heavy Minerals from Selected Holocene Peat-Bog Deposits from the Upper Vistula River Valley, Poland. *Minerals* **2020**, *10*, 9. [CrossRef]
38. Miriello, D.; Bloise, A.; Crisci, G.M.; De Luca, R.; De Nigris, B.; Martellone, A.; Osanna, M.; Pace, R.; Pecci, A.; Ruggieri, N. Non-Destructive Multi-Analytical Approach to Study the Pigments of Wall Painting Fragments Reused in Mortars from the Archaeological Site of Pompeii (Italy). *Minerals* **2018**, *8*, 134. [CrossRef]
39. Huang, E.; Chen, C.H.; Huang, T.; Lin, E.H.; Xu, J.A. Raman spectroscopic characteristics of Mg-Fe-Ca pyroxenes. *Am. Mineral.* **2000**, *85*, 473–479. [CrossRef]
40. Wang, A.; Jolliff, B.L.; Haskin, L.A.; Kuebler, K.E.; Viskupic, K.M. Characterization and comparison of structural and compositional features of planetary quadrilateral pyroxenes by Raman spectroscopy. *Am. Mineral.* **2001**, *86*, 790–806. [CrossRef]
41. Rinaudo, C.; Belluso, E.; Gastaldi, D. Assessment of the use of Raman spectroscopy for the determination of amphibole asbestos. *Mineral. Mag.* **2004**, *68*, 455–465. [CrossRef]
42. Reddy, B.J.; Frost, R.L. Spectroscopic characterization of chromite from the Moa-Baracoa Ophiolitic Massif, Cuba. *Spectrochim. Acta A* **2005**, *61*, 1721–1728. [CrossRef] [PubMed]
43. McKeown, D.A. Raman spectroscopy, vibrational analysis, and heating of buergerite tourmaline. *Phys. Chem. Min.* **2008**, *35*, 259–270. [CrossRef]
44. Bersani, D.; Andò, S.; Scrocco, L.; Gentile, P.; Salvioli-Mariani, E.; Fornasini, L.; Lottici, P.P. Composition of Amphiboles in the Tremolite-Ferro-Actinolite Series by Raman Spectroscopy. *Minerals* **2019**, *9*, 491. [CrossRef]
45. Apopei, A.I.; Buzgar, N. The Raman study of amphiboles. *Geology* **2010**, *56*, 57.
46. Apopei, A.I.; Buzgar, N.; Buzatu, A. Raman and infrared spectroscopy of kaersutite and certain common amphiboles. *Geology* **2011**, *57*, 35–58.
47. Buzatu, A.; Buzgar, N. The Raman study of single-chain silicates. *Geology* **2010**, *56*, 107.
48. Hoang, L.H.; Nguyen, T.M.H.; Chen, X.B.; Minh, N.V.; Yang, I.S. Raman spectroscopic study of various types of tourmalines. *J. Raman Spectrosc.* **2011**, *42*, 1442–1446. [CrossRef]
49. Kloprogge, J.T.; Case, M.H.; Frost, R.L. Raman microscopic study of the Li amphibole holmquistite, from the Martin Marietta Quarry, Bessemer City, NC, USA. *Mineral. Mag.* **2001**, *65*, 775–785. [CrossRef]
50. Andò, S.; Garzanti, E. Raman spectroscopy in heavy-mineral studies. *Geol. Soc. Spec. Publ.* **2014**, *386*, 395–412. [CrossRef]
51. D'Ippolito, V.; Andreozzi, G.B.; Bersani, D.; Lottici, P.P. Raman fingerprint of chromate, aluminate and ferrite spinels. *J. Raman Spectrosc.* **2015**, *46*, 1255–1264. [CrossRef]
52. Chukanov, N.V.; Vigasina, M.F. *Vibrational (Infrared and Raman) Spectra of Minerals and Related Compounds*; Springer International Publishing: Cham, Switzerland, 2020. [CrossRef]
53. Kos, S.; Dolenec, M.; Lux, J.; Dolenec, S. Raman Microspectroscopy of Garnets from S-Fibulae from the Archaeological Site Lajh (Slovenia). *Minerals* **2020**, *10*, 325. [CrossRef]
54. Maftei, A.E.; Buzatu, A.; Damian, G.; Buzgar, N.; Dill, H.G.; Apopei, A.I. Micro-Raman—A tool for the heavy mineral analysis of gold placer-type deposits (Pianu Valley, Romania). *Minerals* **2020**, *10*, 988. [CrossRef]

55. Zhai, K.; Xue, W.H.; Wang, H.; Wu, X.; Zhai, S.M. Raman spectra of sillimanite, andalusite, and kyanite at various temperatures. *Phys Chem Min.* **2020**, *47*, 23. [CrossRef]
56. Fu, M.H.; Dai, J.J.; Zhao, L.X. A Study on the Raman Spectral Characteristics of Garnet from the Jiama Copper Polymetallic Deposit in Tibet. *Minerals* **2022**, *12*, 1578. [CrossRef]
57. Borromeo, L.; Andò, S.; Bersani, D.; Garzanti, E.; Gentile, P.; Mantovani, L.; Tribaudino, M. Detrital orthopyroxene as a tracer of geodynamic setting: A Raman and SEM-EDS provenance study. *Chem. Geol.* **2022**, *596*, 120809. [CrossRef]
58. Limonta, M.; Andò, S.; Bersani, D.; Garzanti, E. Discrimination of Clinozoisite-Epidote Series by Raman Spectroscopy: An application to Bengal Fan Turbidites (IODP Expedition 354). *Geosciences* **2022**, *12*, 442. [CrossRef]
59. Sundararajan, M.; Rejith, R.G.; Renjith, R.A.; Mohamed, A.P.; Gayathri, G.S.; Resmi, A.N.; Jinesh, K.B.; Loveson, V.J. Raman-XPS spectroscopic investigation of heavy mineral sands along Indian coast. *Geo-Mar. Lett.* **2021**, *41*, 22. [CrossRef]
60. do Nascimento-Dias, B.L. Overview about Raman spectroscopy of types of olivine group minerals: A brief review. *J. Raman Spectrosc.* **2022**, *53*, 1942–1946. [CrossRef]
61. Torre-Fdez, I.; García-Florentino, C.; Huidobro, J.; Coloma, L.; Ruiz-Galende, P.; Aramendia, J.; Castro, K.; Arana, G.; Madariaga, J.M. Characterization of olivines and their metallic composition: Raman spectroscopy could provide an accurate solution for the active and future Mars missions. *J. Raman Spectrosc.* **2023**, *54*, 340–350. [CrossRef]
62. Zheira, G.; Masoudi, F.; Rahimzadeh, B. Identification of Fe3+ content in epidote from Varan, Urumieh-Dokhtar magmatic arc, Iran: Using FTIR and Raman spectroscopy. *Iran. J. Earth Sci.* **2022**, *14*, 131–139. [CrossRef]
63. Lafuente, B.; Downs, R.T.; Yang, H.; Stone, N. The power of databases: The RRUFF project. In *Highlights in Mineralogical Crystallography*; W. De Gruyter: Berlin, Germany, 2015; pp. 1–30.
64. Komar, P.D. The entrainment, transport and sorting of heavy minerals by waves and currents. In *Developments in Sedimentology*; Mange, M.A., Wright, D.T., Eds.; Elsevier: Amsterdam, The Netherlands, 2007; Volume 58, pp. 3–48.
65. Cascalho, S.; Fradique, C. The Sources and Hydraulic sorting of heavy minerals on the northern portuguese continental margin. In *Developments in Sedimentology*; Mange, M.A., Wright, D.T., Eds.; Elsevier: Amsterdam, The Netherlands, 2007; Volume 58, pp. 75–107.
66. Mason, B.; Donnay, G.; Hardie, L.A. Ferric tourmaline from Mexico. *Science* **1964**, *144*, 71–73. [CrossRef] [PubMed]
67. Arnaudov, V.; Petrussenko, S.; Karov, C. Buergerite in pegmatites from the Plana Cretaceous pluton, Western Bulgaria. *Geochem. Mineral. Pet.* **2002**, *39*, 75–80.
68. Augustsson, C.; Bahlburg, H. Provenance of late Palaeozoic metasediments of the Patagonian proto-Pacific margin (southernmost Chile and Argentina). *Int. J. Earth Sci.* **2008**, *97*, 71–88. [CrossRef]
69. Mange, M.A.; Wright, D.T. *Heavy Minerals in Use*; Elsevier: Amsterdam, The Netherlands, 2007.
70. Rodriguez Fernandez, R.; Oliveira, T.J. Mapa Geologico de Espana y Portugal—Geological Map of Spain and Portugal 1:1,000,000 Scale. Available online: https://info.igme.es/visor/ (accessed on 31 May 2024).
71. Pettijohn, F.J.; Potter, P.E.; Siever, R. *Sand and Sandstone*; Springer: New York, NY, USA, 1972. [CrossRef]
72. Hubert, J.F. A zircon-tourmaline-rutile maturity index and the interdependence of the composition of heavy mineral assemblages with the gross composition and texture of sandstones. *J. Sediment. Res.* **1962**, *32*, 440–450. [CrossRef]
73. Tangari, A.C.; Le Pera, E.; Andò, S.; Garzanti, E.; Piluso, E.; Marinangeli, L.; Scarciglia, F. Soil-formation in the central Mediterranean: Insight from heavy minerals. *Catena* **2021**, *197*, 104998. [CrossRef]
74. Nowicki, T.E.; Moore, R.O.; Gurney, J.J.; Baumgartner, M.C. Diamonds and associated heavy minerals in kimberlite: A review of key concepts and applications. In *Developments in Sedimentology*; Mange, M.A., Wright, D.T., Eds.; Elsevier: Amsterdam, The Netherlands, 2007; Volume 58, pp. 1235–1267.
75. Neilson, S.; Grütter, H.; Pell, J.; Grenon, H. The evolution of kimberlite indicator mineral interpretation on the Chidliak project, Baffin Island, Nunavut. In Proceedings of the International Kimberlite Conference, Bangalore, India, 6–11 February 2012.
76. Pell, J.; Russell, J.K.; Zhang, S.X. Kimberlite emplacement temperatures from conodont geothermometry. *Earth Planet. Sci. Lett.* **2015**, *411*, 131–141. [CrossRef]